Nonlinear dynamics of dispersion managed breathers in Gaussian Ansatz approximation

R. Paškauskas
The Niels Bohr Institute,
Blegdamsvej 17,
DK-2100 Copenhagen, Ø
Denmark
(February 2, 2000)

In this term paper we make a brief investigation of nonlinear dynamics generated by one of probably many possible truncations of Nonlinear Schrödinger equation (NLS) by examining Poincare maps. That is - following [1] we assume Gaussian Ansatz of pulse envelope, and truncate NLS thus producing two coupled nonlinear ODE's. Then we analyze rezulting system of ODE's in the case of piecewise constant dispersion.

Our interest is in pulse propagation through optical fibers. Dynamics of electric field envelope in this case is described by NLS:

$$\imath \frac{\partial A}{\partial z} + \frac{g}{2}\frac{\partial^2 A}{\partial t^2} + \frac{\omega n_2}{c}|A|^2 A = 0 \tag{1}$$

which conserves energy $\int |A|^2 dt$, and for a medium with Kerr nonlinearity, characterized by the nonlinear coefficient n_2, and taking no transversal effects and energy loss into account. Here A is complex amplitude of electric field, ω - is central frequency, c - speed of light, g - group velocity dispersion (GVD). Let us normalize quantities to standart nondimensional form. First we normalize complex amplitude to its peak value, e.g. $A = A_0 Q$. Then introduce Nonlinear length L_n

$$L_n = \frac{c}{A_0^2 \omega n_2} \tag{2}$$

and normalize z to L_n: $Z = z/L_n$, and normalize time t to $T = t/\tau$, $\tau = T_0/\kappa$, where T_0 is FWHM of the pulse. Now NLS reads as:

$$\imath \frac{\partial Q}{\partial Z} + \frac{L_n g}{2\tau^2}\frac{\partial^2 Q}{\partial T^2} + |Q|^2 Q = 0 \tag{3}$$

The dispersion coefficient σ,

$$\sigma = \frac{L_n g}{\tau^2} \tag{4}$$

will be taken to be piecewise constant function of Z, may be set to be of unit magnitude. Gaussian ansatz, which we assume, states that shape of a pulse is Gaussian at each point Z to a given accuracy. Then we seek for a solution of the form

$$Q(Z,T) = \sqrt{\eta(Z)} e^{-(\eta(Z)\kappa T)^2 + \imath\beta(Z)\kappa^2 T^2 + \imath\phi(Z)/2} \tag{5}$$

In this ansatz energy does not depend on Z, i.e. it is conserved. Q may be regarded as a field variable, NLS being equations of motion generated by the following action integral

$$S = \int dT dZ \mathcal{L}(Q^*, \partial_T Q^*, \partial_Z Q^*) \tag{6}$$

where Lagrangian density $\mathcal{L}$ is:

$$\mathcal{L} = \imath \left(Q \frac{\partial Q^*}{\partial T} - Q^* \frac{\partial Q}{\partial T} \right) + \sigma(Z) \left| \frac{\partial Q}{\partial T} \right|^2 - |Q|^4 \tag{7}$$

In this way NLS may be obtained by Euler-Lagrange equation

$$\left(\frac{\partial}{\partial Q^*} - \frac{\partial}{\partial Z}\frac{\partial}{\partial(\partial_Z Q^*)} - \frac{\partial}{\partial T}\frac{\partial}{\partial(\partial_T Q^*)} \right) \mathcal{L} = 0 \tag{8}$$

Taking this equation with respect to Q produces complex conjugate equation to NLS. We will use Lagrangian formalism to derive equations of motion (EOM) for free parameters η, β, ϕ. Lagrangian is

$$L = \int dT\, \mathcal{L} \tag{9}$$

We have evaluated it to be

$$L = \frac{d\phi}{dZ} \int dT |Q|^2 + \left(\kappa^2 \frac{d\beta}{dZ} + 4\sigma\kappa^4(\eta^4 + \beta^2) \right) \int dT\, |Q|^2 T^2 - \int dT |Q|^4 \tag{10}$$

Using given form of Q we evaluate integrals

$$\int dT\,|Q|^2 = \frac{1}{\kappa}\sqrt{\frac{\pi}{2}} \tag{11}$$

$$\int dT|Q|^2T^2 = \sqrt{\frac{\pi}{2}}\frac{1}{4\kappa^3\eta^2} \tag{12}$$

$$\int dT|Q|^4 = \sqrt{\pi}\frac{\eta}{2\kappa} \tag{13}$$

By substituting these expressions into Lagrangian, we get

$$L = \frac{d\phi}{dZ} + \frac{1}{4\eta^2}\frac{d\beta}{dZ} + \sigma\kappa^2(\eta^2 + \frac{\beta^2}{\eta^2}) - \frac{1}{\sqrt{2}}\eta \tag{14}$$

The phase term ϕ doesn't play any role in classical dynamics, because action depends only on it's values at the end points and it's variations give zero contribution.We may omit it. Secondly we will normalize variables

$$\sigma \leftarrow \frac{4\kappa^2}{\sqrt{2}}\sigma \tag{15}$$

$$Z \leftarrow \sqrt{2}Z \tag{16}$$

Now the Lagrangian is as follows

$$L(\eta, \beta, \frac{d\eta}{dZ}, \frac{d\beta}{dZ}) = \frac{1}{\eta^2}\frac{d\beta}{dZ} + \sigma(\eta^2 + \frac{\beta^2}{\eta^2}) - 2\eta \tag{17}$$

The Lagrange equations were used to obtain EOM:

$$p_\eta = \frac{\partial L}{\partial(\partial_Z\eta)} = 0 \tag{18}$$

$$p_\beta = \frac{\partial L}{\partial(\partial_Z\beta)} = \frac{1}{\eta^2} \tag{19}$$

$$\frac{1}{2}\frac{dp_\eta}{dZ} = -\frac{1}{\eta^3}\frac{d\beta}{dZ} + \sigma(\eta - \frac{\beta^2}{\eta^3}) - 1 = 0 \tag{20}$$

$$\frac{dp_\beta}{dZ} = \frac{2\sigma\beta}{\eta^2} \tag{21}$$

Solving these equations for derivatives $\frac{d\eta}{dZ}, \frac{d\beta}{dZ}$ yelds us EOM which is a system of two ODE's:

$$\frac{d\eta}{dZ} = -\sigma\eta\beta \tag{22}$$

$$\frac{d\beta}{dZ} = \sigma(\eta^4 - \beta^2) - \eta^3 \tag{23}$$

This system has one integration constant - energy, E which is found by constructing Hamilton's function. We construct Hamiltonian as

$$H = \frac{1}{\eta^2}\frac{d\beta}{dZ} - L = E \tag{24}$$

In this way we obtain that E is

$$E = -\sigma(\eta^2 + \frac{\beta^2}{\eta^2}) + 2\eta \tag{25}$$

The equation of separatrix is given by

$$\beta^2 = \eta^2(\frac{2\eta}{\sigma} - \eta^2) \tag{26}$$

So, we may eliminate one variable using integration constant and have only one ODE left to integrate. Integration may be done analytically and semiexplicit expressions for variables η, β are obtainable in the form $Z = Z(\eta, \beta)$, for details one is referenced to [2]. In this term paper we, nevertheless, obtain most of the results using Runghe Kutta routine to integrate both EOM.

The two dimensionality of the problem might be manifested if we'd consider Hamiltonian EOM. We may construct from equations (18) through (21) and (25) the Hamiltonian formalism, which is essentially two dimensional,

$$H(p,q) = \sigma(\frac{1}{p} + pq^2) - \frac{2}{\sqrt{p}}, \tag{27}$$

where canonical variables p and q are defined as

$$q \equiv \beta \tag{28}$$

$$p = \frac{1}{\eta^2}, \tag{29}$$

yelding another set of EOM

$$\frac{dp}{dZ} = 2\sigma pq \tag{30}$$

$$\frac{dq}{dZ} = \sigma(q^2 - \frac{1}{p^2}) + \frac{1}{p^{3/2}}, \tag{31}$$

which are equivalent to (22) and (23). Though we will find easier to integrate the system of equation (22) and (23), which is by the way non Hamiltonian in variables η and β.

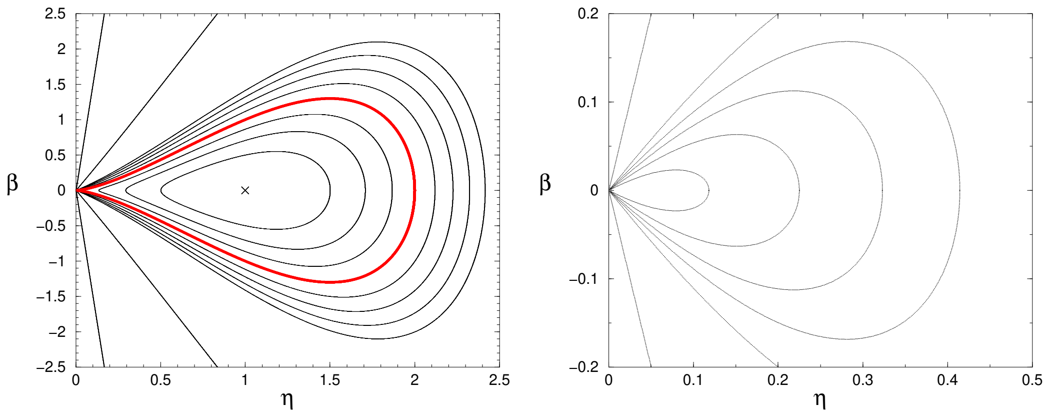

(a) $\sigma = \sigma_+$

(b) $\sigma = -\sigma_-$

FIG. 1. The family of integral curves in two cases of σ flow. Parameters were taken to be $\sigma_+ = \sigma_- = 1$.

We plotted some trajectories for a constant dispersion σ being positive and negative respectively in fig(1). Several trajectories of differrent energy (25) are plotted. The flow in forward direction is carried "counterclockwise" in case of $\sigma = \sigma_+ > 0$, and "clockwise" in case $\sigma = -\sigma_- < 0$. The case σ_-, medium acts as defocusing and this effect in combination with dispersion of the pulse results in its eventual spreading. Thus $\eta \to 0$ as $Z \to \infty$. In case of σ_+ there exists a set of initial conditions when solutions are periodic.$\sigma > 0$ is necessary condition for existanse of periodic solutions. This may be explained in the way that dispersive spreading is compensated by compression due to self focusing action of medium. The set of periodic points is determined by inequality $E(\eta, \beta) < 0$ (see equation 25) and the equation of separatrix, curve that separates periodic solutions from the other nonperiodic ones is equation $E(\eta,\beta)=0$. When $\sigma<0$ there is one degenerate equilibrium point $(0,0)$. Every trajectory eventually ends on it. When $\sigma>0$ this point still exists as a fixed and degenerate one, but in addition there's another equilibrium point $(1/\sigma,0)$. This point is center, and periodic trajectories "spin" around it. It's Liapunov exponent is a pair of imaginary numbers $\pm\imath/\sigma$.

Dynamics in (η,β) plane is symmetric with respect to involution $Z\to -Z$, and $\beta\to-\beta$ and the flow is reversible. That basically suggests, if we evolve from a given starting point (η_0,β_0) forward some distance (say Z') and end in (η_1,β_1) and plot resulting trajectory in plane (η,β), then to obtain backward evoluton, for the same Z' from another starting point $(\eta_0,-\beta_0)$, we just plot mirror image with respect to η axis of the former trajectory and arrow of velocity of backward evolution pointing in the backward direction. It is obvious that trajectory will "end" at $(\eta_1,-\beta_1)$. What will happen if we take $\beta_0=0$? We will have forward evolution from 0 to β_1 and backward evolution from 0 to $-\beta_1$, or due to reversibility of this flow, forward evolution $-\beta_1\to\beta_1$. Let's say we want to find a loop - a periodic solution. According to previous discussion we need to set $\beta_1=0$, so that we have evolution $0\to 0$ and this problem is solved. This result may seem almost trivial, especially after a glance to figures which illustrate σ_+ flow (fig1), as indeed periodic solutions cross η axis at 2 points, just as follows from discussion. But the merit of the discussion is that its results hold in a somewhat less trivial case of piecewise dispersion.

When there's only piecewise constant periodic dispersion management, the same argument holds. There is a natural way to describe dynamics by mapping the trajectory in intervals of period of dispersion management. It is a convenient choise to map middle of each interval with negative dispersion. Our (see also [2]) choise of dispersion map is following

$$\sigma(Z)=\begin{cases} -\sigma_- & : \quad -(Z_-+Z_+)<Z<-Z_+ \\ \sigma_+ & : \quad -Z_+<Z<Z_+ \\ -\sigma_- & : \quad Z_+<Z<Z_-+Z_+ \end{cases} \tag{32}$$

And $\sigma(Z)$ has a period $2(Z_++Z_-)$. With this dispersion map, the map of dynamics is still involution invariant. That is, if we make forward evolution ("to the right") from the center of interval with negative dispersion (the point of mapping) with initial point (η_0,β_0), evolve system until the middle of the nearest interval ("to the right") with positive dispersion (half a period - half map) to resulting point (η_1,β_1) and map these two points, then the similar map from $(\eta_0,-\beta_0)$ by backward evolution ("to the left") will map to $(\eta_1,-\beta_1)$. In accordance with [2] we will denote operation that evolves given initial set Ω, say, distance Z_- of σ_- flow as T_- (T_+ in case of evolution Z_+ carried by σ_+) and ending set is eventually $T_-\Omega$ (alternatively $T_+\Omega$). In this notation operation of Poincare mapping is $P=T_-T_+T_+T_-$. The strategy of finding a periodic orbit (only 1-cycle) is apparent. In analogy to the previous discussion of continuous flow, the point $(\eta_0,0)$ will map to (η_1,β_1) by forward evolution, and to $(\eta_1,-\beta_1)$ by backward evolution. So the poincare map of the point $(\eta_1,0)$ will map to $(\eta_1,0)$ provided the half-map of this point is $(\eta_2,0)$. In particular one may make a half-map of a set $\mathcal{R}$, defined as $\mathcal{R}=\{(\eta,\beta):\beta=0\}$. The point of intersection of "Poincare half-map" $T_+T_-\mathcal{R}$ with $\mathcal{R}$ lies on a periodic orbit. In case of 1-cycle there are no fixed points off the $\mathcal{R}$. It follows from requirement that each periodic trajectory be involution invariant and from the necessity to construct the cycle using only two segments [1] of trajectories, one from each of $\sigma_\pm$ flows. But as can be seen from 1 any two segments of trajectories intersect at only two (or none) symmetric points (not mentioning a trivial intersection at (0,0)). That restricts the family of all length periodic orbits to relatively few periodic orbits that have definite symmetry, such as orbit has to cross η axis at right angle, have mirror symmetry etc. This requirement hold for all length cycles, thus making all the cycles topologically quite similar.

Assume for the moment that σ_+,σ_-,Z_- are given fixed values. We shall vary Z_+. Let's start evolving a "test point" with some initial value $x_0=(\eta_0,\beta_0=0)$ and propagate it to $x_1=T_-x_0$. Either x_1 lies inside of the separatrix of σ_+ flow, or outside it. If it is inside then the following evolution under subsequent σ_+ flow will circulate this "test point" around fixed point eventualy making it hit $\mathcal{R}$. The period of periodic solution in σ_+ flow is given by the formula

$$T(\delta) = \frac{2\pi\sigma_+}{(1-\delta^2)^{3/2}} \tag{33}$$

where δ is given by $\eta_2 = (1+\delta)/\sigma_+$, and η_2 is the point of intersection of orbit with $\mathcal{R}$ to the right from fixed point $1/\sigma_+$ (for derivation see [2]). The period changes monotonously with increasing δ and reaches infinity at separatrix ($\delta = 1$). Indeed me may see that inside the separatrix test point is carried away from the origin monotonously even by the previous σ_- flow. There is also only one point where image $T_-\mathcal{R}$ crosses the separatrix. If we set initial point such, that ($\eta_0 \ll 1, \beta_0 = 0$) then from (23) we may approximate

$$\frac{d\beta}{dZ} \approx \beta^2 - \eta^3 \tag{34}$$

considering η to be a constant. Here we have aproximated (23) to the least power in η and put $\sigma_- = 1$. Coresponding to the solution of this ODE respecting initial values

$$\beta^2 = \eta^3 \sinh^2 Z \tag{35}$$

Inserting this expression into (22), and assuming that $Z \ll 1$ yelds equation

$$\frac{d\eta}{dZ} = -\eta^{5/2} Z \tag{36}$$

Expansion of the solution of this equation to the leading term in Taylor series gives expression

$$\eta = \eta_0(1 - \frac{1}{2}\eta_0^{3/2} Z^2) \tag{37}$$

Limiting cases (37, 35) indicate that the map $x = T_- x_0$ is inside a separatrix (26) for small η_0. Next we may show how does asymptotic map behaves in case when $\eta_0 \gg 1$. For that reason we make another approximation

$$\frac{d\beta}{dZ} \approx \beta^2 - \eta^4 \tag{38}$$

Solution yelds

$$\beta = -\eta^2 \sinh(Z) \tag{39}$$

Then is clear that

$$\frac{d\eta}{dZ} = -\eta^3 \sinh Z \tag{40}$$

And solution to this equation yelds

$$\eta^2 = \frac{\eta_0^2}{1 - 4\eta_0^2 \sinh^2(Z/2)} \tag{41}$$

And by this we see that

$$\beta = -\frac{\eta_0^2 \sinh Z}{1 - 4\eta_0^2 \sinh^2(Z/2)} \tag{42}$$

And in the limit $\eta_0 \to \infty$ we get asymptotic mapping

$$\eta \to 1/Z^2 \tag{43}$$
$$\beta \to -1/Z, \tag{44}$$

which lies outside separatrix. Thus the map $T_-\mathcal{R}$ crosses the separatrix at one point only. An important conclusion from these considerations for us is that map $T_- x_0$ of sufficiently small η_0 lies inside the separatrix and that inside it β is a monotonously decreasing function of Z. Then part of the map $x = T_- x_0$ inside separatrix crosses some of the periodic solutions of T_+ operator and thus for sufficiently large Z_+ there is η_0 such that $T_+T_-x_0$ crosses $\mathcal{R}$ also such x_0 which doesn't cross it,so there is x_0 such that $T_+T_-x_0 \subset \mathcal{R}$. For small Z_+ there are indeed no 1-cycles. But as Z_+ increases, there comes the point when one "test point" is being mapped to $\mathcal{R}$ then after another Z_+ is reached there will be two new such points and so on. This mechanism creates bifurcation[1] points with increasing Z_+. The larger Z_+ the more crossings $\mathcal{R} \cap T_+T_-\mathcal{R}$ there are. Thus we see that every fixed point belongs to set $\mathcal{R}$ and number of fixed points increases with increasing ratio Z_+/Z_-. Figure 2 will serve to illustrate these conslusions. We plotted map of T_-x_0 and may observe that a segment of this map lies inside separatrix of the σ_+ flow. Existence of this segment is a necessary condition that periodic orbits may be.

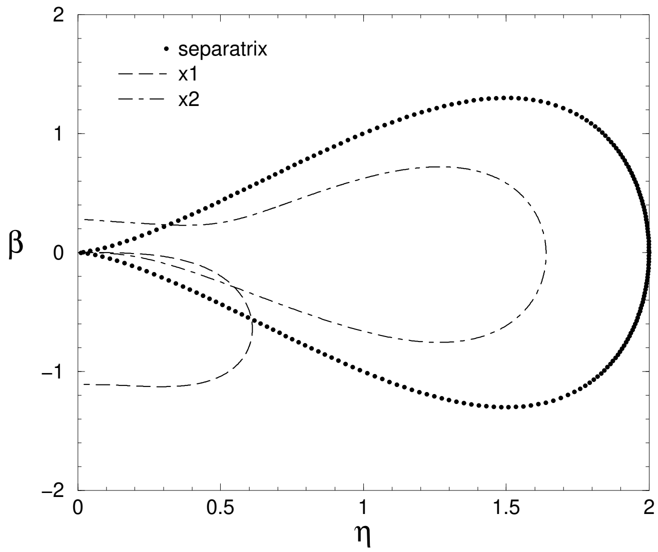

FIG. 2. Images of $\mathcal{R}$ under $T_\pm$. Long dashed line is $x1 = T_-\mathcal{R}$. Dash-dotted line is $x2 = T_+T_-\mathcal{R}$. Circled line is separatrix. We set parameters to be $\sigma_+ = \sigma_- = Z_- = 1, Z_+ = 5$

In the next figure we should find the sequence of pictures of a given map for different parameter values. In each of this region a different type of 1-cycles may be found. Each subsequent region contains all the cycles from previous regions and an additional pair of 1-cycles. We may remind that if the map $T_+T_-x_0$ crosses the abscissae then there is a completely determined 1-cycle. So that crossing equivalently coresponds to a cycle.

To seek a fixed point one may use the following simple algorithm: first find intersection $x = \mathcal{R} \cap T_+T_-\mathcal{R}$ and evolve x backward $x_0 = (T_+T_-)^{-1}x$. But due to involution invariance $(T_+T_-)^{-1} = T_-T_+$. After finding the necessary root there evolution should be performed, which will bring some errors no mater how accurately the root was found. The resulting "fixed point" may be used as an execellent starting guess further to be yet improved by the Newton routine.

[1] bifurcation in the sense that there is a critical parameter values when the transition to two 1-cycles for given parameters occur. This bifurcation is not period doubling.

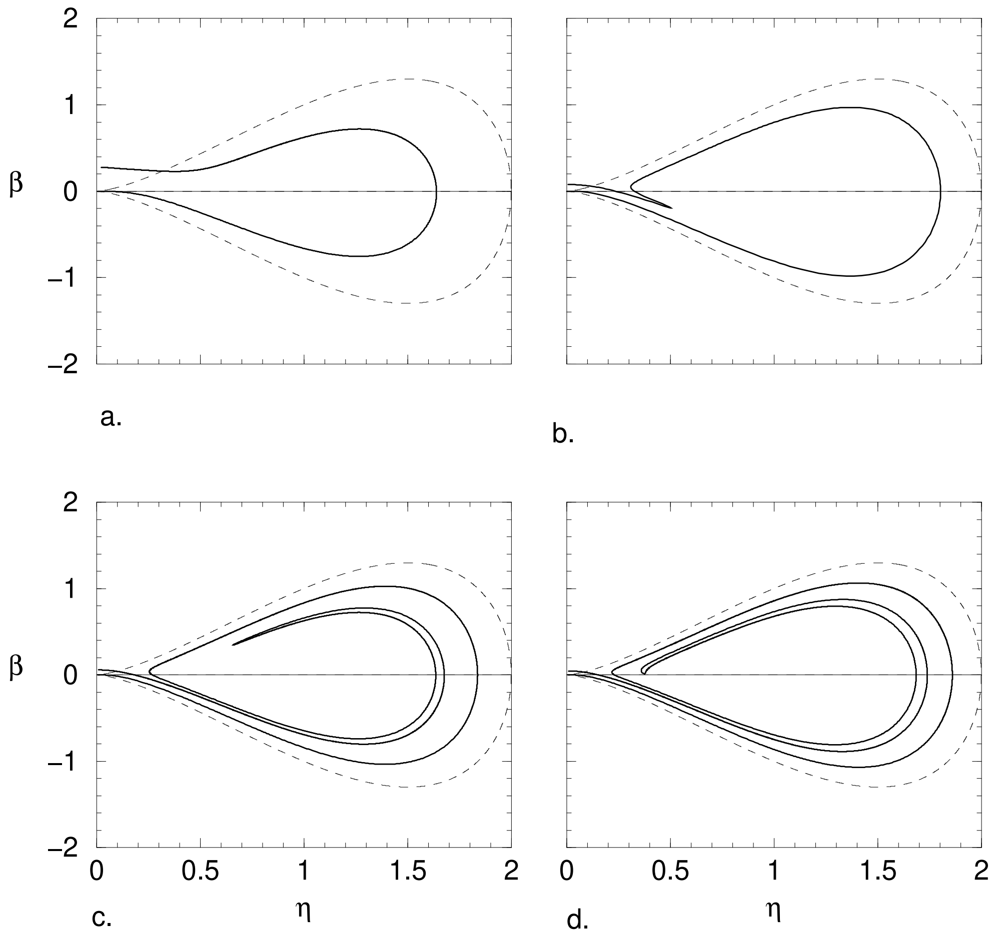

FIG. 3. Images of $T_+T_-\mathcal{R}$ for different parameter Z_+ values. a:$Z_+ = 5$, b:$Z_+ = 10$, c:$Z_+ = 20$, d:$Z_+ = 25$. Bifurcations occur in the form of number of crossings $\mathcal{R} \cap T_-T_+\mathcal{R}$, which increases with increasing Z_+ from 1 in (a) case to 5 in (c) case. The (d) case shows a situation very close to bifurcation. Here we have set $Z_- = \sigma_- = \sigma_+ = 1$. A dashed line plots separatrix of σ_+ flow. Also $\mathcal{R}$ is plotted.

In the following pages we have plotted several Poinare maps. Each of them represents dynamics of trajectories started from several different initial values. The initial values were selected to be on the line $\beta = 0$, but otherwise distributed homogeniously on this line. The chaotic solutions start to appear from the very first picture i.e. as soon as continuous flow σ is replaced by a piecewise constant map $\sigma_\pm$. When there's a piecewise map the "test point" which we've started to evolve in one region keeps it's energy during this interval, but at the edge of crossing with interval of different sign of σ it suddently changes energy, because formaly the functional dependence of energy is different right after the edge. Then if it is not "sufficiently" close to a periodic trajectory, this point may wander a rather large "distance" in both η and β from it's former energy shell, so at the next edge it will suddently change its energy in a way which is faintly constrained. That is why the dynamics in practise may be chaotic. If one of intervals is quite narrow, then this interval changes coordinates of our point by a small amount and trajectory drifts away by a small amount. Then averaging may be applied to obtain an approximate result, which states that the point behaves as if in the field of constant, but averaged dispersion. This is indeed the case in situation, showed on fig 4. The dynamics is similar to unperturbed one in field of constant dispersion

$$\bar{\sigma} = \frac{Z_+\sigma_+ - Z_-\sigma_-}{Z_+ + Z_-}, \tag{45}$$

which in this case is $\bar{\sigma} = 1/3$. For example fixed point of a flow is given in terms $\eta_{fixed} = 1/\bar{\sigma} = 3$, so in the averaged case it gives rather precise estimate (see fig 4).

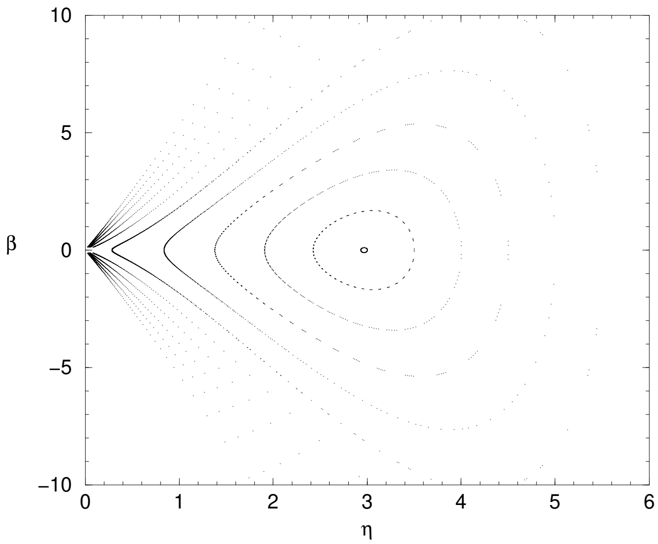

FIG. 4. A Poincaré map for parameters $Z_{-} = 0.01$, $Z_{+} = 0.02$.

The Poincaré map as in fig 5 shows increasing regions of chaoticity. We may notice that trajectories in the vicinity of a periodic point form closed orbits, but the regions of chaos spread. Also new type of motion may be observed, as in Poincare map it forms chains of eliptic followed by hyperbolic points. Eliptical points of this type (see also zoom in figs 8 and 9) are fixed points of longer than 1-cycles. Though the elliptical points seem to have isolated curves around them, in fact dynamics on neither these curves, nor fixed points themselves is bound inside the region and thus cannot be contracted to a point. A periodic orbit starting at one of these points will visit all of the fixed points in a given family situated around the "proper" 1-cycle fixed point, which is $\eta \approx 2.10$.

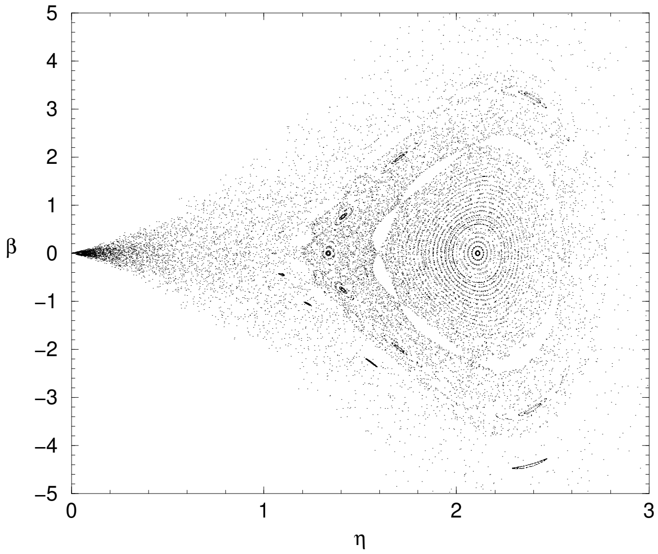

FIG. 5. A Poincaré map for parameters $Z_{-} = 0.01$, $Z_{+} = 0.1$.

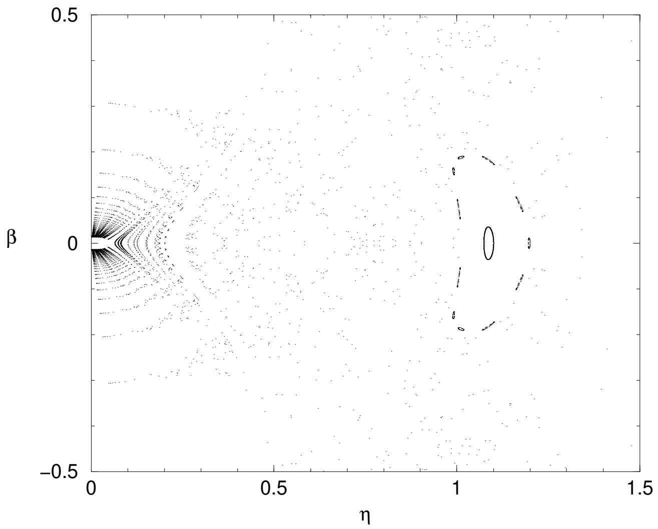

FIG. 6. A Poincaré map for parameters $Z_{-} = 0.01$, $Z_{+} = 1.0$.

The fig 7 shows that the bifurcation has occured somewhere $0.1 < Z_{+} < 1.0$, between parameters of this figure and of fig 6, as here we may see a brand new pair of 1-cycle fixed points. Chaotic regions outside fixed points inrease.

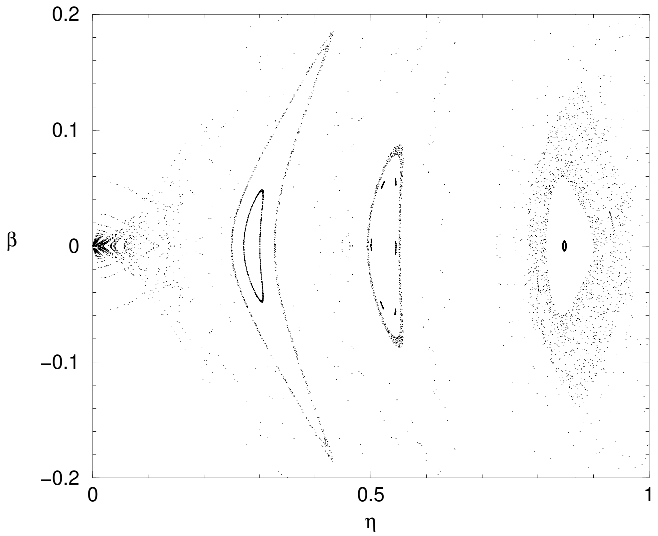

FIG. 7. A Poincare map for parameters $Z_{-} = 0.01$, $Z_{+} = 10$. A fixed point pair is created around $\eta \approx 0.3$ and $\eta \approx 0.55$.

In the following two figures we have enlarged the Poincaré map of fig 5 and shown parts of regions with elliptic and hyperbolic points[2].

---

[2]In the first of these figures 8 map looks somewhat asymetrical, but this is because we had to skip every n-th point in our data file to keep this paper within reasonable size limits

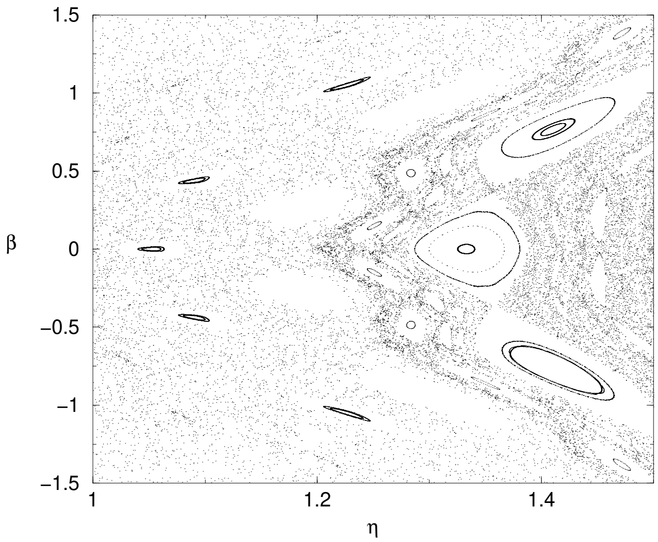

FIG. 8. A zoom in of the Poincaré map of fig 5.

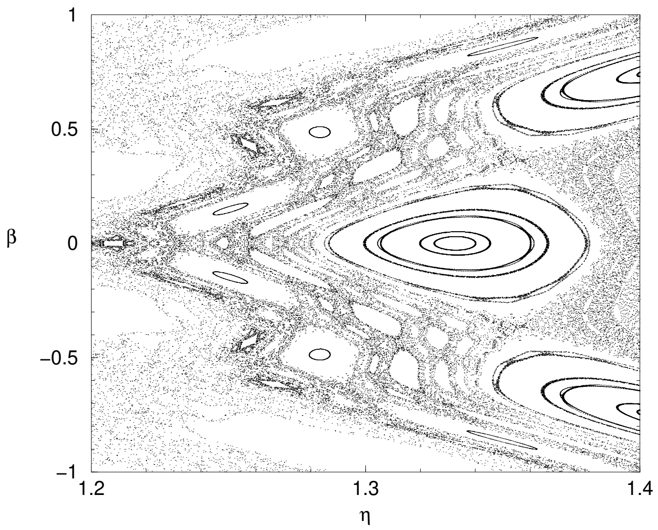

FIG. 9. A zoom in of the Poincaré map of fig 8.

The mechanism of sudden change in energy as described above may suggest some similarity with a model of a kicked rotator, treated in many books, for instance in [4]. It is easy to notice that Poincaré maps in the cited book are visualy quite resemblant to ours in for example fig 9.

Next we will draw our attention to examining stabilities of cycles as functions of parameters Z_+ and Z_-, because, as we have seen these parameters or a function of them will determine the structure of the Poinacaré map and number of cycles. As means of finding periodic trajectories we shall derive a modification of the Newton routine, where we shall use some of particular properties of our system, decsribed by (22) and (23). For general methods and various examples of Newton routine one could consult [3]. We use the following formalism: our map is denoted as

$$\eta_{n+1} = f_1(\eta_n, \beta_n) \tag{46}$$

$$\beta_{n+1} = f_2(\eta_n, \beta_n). \tag{47}$$

The fixed point set is

$$\eta_* = f_1(\eta_*, \beta_*) \tag{48}$$
$$\beta_* = 0. \tag{49}$$

Linearization of functions

$$F_1 = \eta_{n+1} - f_1(\eta_n, \beta_n) \tag{50}$$
$$F_2 = \beta_{n+1} - f_2(\eta_n, \beta_n) \tag{51}$$

around a fixed point $F_1^* = F_2^* = 0$ yelds equations

$$\eta_{n+1} = f_1(\eta_n, 0) + \frac{\partial F_1}{\partial \eta_*}(\eta_n - \eta_*) \tag{52}$$
$$\beta_{n+1} = f_2(\eta_n, 0) + \frac{\partial F_2}{\partial \eta_*}(\eta_n - \eta_*), \tag{53}$$

where we shall set $\eta_* = \eta_n + \delta\eta$ and $\beta_{n+1} = 0$ and arrive at equation

$$\eta_{n+1} = f_1(\eta_n, 0) - f_2(\eta_n, 0)\frac{\partial_{\eta_*} F_1}{\partial_{\eta_*} F_2} \tag{54}$$

We shall use that derivatives in the second term on lefthand side of the last equation are matrix elements of jacobian of transformation from fixed point to point with index $n+1$ or to the first order in $\delta\eta$ we may take them to be

$$\partial_{\eta_*} F_1 \approx J_{\eta,\eta} \tag{55}$$
$$\partial_{\eta_*} F_2 \approx J_{\beta,\eta}. \tag{56}$$

Thus the final form of the equation we've tried to derive is

$$\eta_{n+1} = f_1(\eta_n, 0) - f_2(\eta_n, 0)\frac{J_{\eta,\eta}}{J_{\beta,\eta}}. \tag{57}$$

We may mention that case for the last formula to diverge is rather improbable when the first guess is made, because if this would be the case one would correctly conclude that mapping was paralel to η axis, but if this was the case then the initial point was the fixed point, which would have yelded $f_2 = 0$, so that only case when divergency could occur would be due to second order effects in $\delta\eta$. To interpret the formula (57) we may consider next picture: assume we start from nearby of the fixed point with displacement $\delta\eta$ in the horizontal direction, as we may use the result of previous discussion that $\beta_* = 0$. Then after the linear transport we found ourselves at (f_1, f_2), i.e. carried away from $\beta = 0$ by amount $J_{\beta,\eta}\delta\eta$ and carried horizontally by amount $J_{\eta,\eta}\delta\eta$. Thus our guess of a fixed point will be that (of course) $\beta_* = 0$, which yelds $\delta\eta = f_2/J_{\beta,\eta}$, and $\eta_* = f_1 - J_{\eta,\eta}\delta\eta$. This guess is precisely what is stated by (57) equation.

We have tested our formula by numerical simulations. Firstly we demonstrate convergency of the routine. We've chosen parameters $Z_+ = 0.1$ and $Z_- = 0.01$. The coresponding Poincaré map is pictured in fig 5 where we may see a fixed point close to $\eta = 2.1$. We may choose initial guess, for example $\eta = 2.2$ (5 % away), and check it's convergency. We performed simulation and the results are in the table. We put there results produced by a given guess. First we guess η, then calculate map $P(\eta, \beta)$, it's jacobian, absolute value of jacobian's eigenvalue ($|\lambda|$), and correction $\delta\eta$. Then take $\eta \to \eta + \delta\eta$ and repeat the same procedure.

N	η	β	$\|\lambda\|$	$\delta\eta$
1	2.133265	0.434145	0.954847	-0.014717
2	2.112348	0.043041	0.995614	-0.003253
3	2.109017	0.000546	0.999946	-0.000044
4	2.108973	0.000003	1.000001	0.000000
5	2.108973	0.000003	1.000001	0.000000

TABLE I. Test results of the Newton routine

Iterations converge rather fast, even with worse than this initial guesses until some point. We may see that the last two rows in the table don't differ. I have a version that this residual error is due to algorithm of integration. For I used linear interpolation to connect two regions $\sigma_\pm$ which is only linear in the stepsize, and indeed I noticed that this so called "residual error" decreases slowly when integration stepsize is being reduced.

We have programed a routine to inplement (57) formula. By means of it we were able to find periodic orbits and their stabilities, given a good initial guess. It was applicable to calculate period doubling bifurcation diagram. We chose $Z_- = 1$ to be a constant and varied Z_+. Results of data revealed that 1-cycles before the bifurcation point have two real stability eigenvalues and their product is very close to unity. When plotted, these solutions looked to be stable, persisting to at least 10 periods. But if developed further, the periodic orbits decay into chaotic motion. Because one of the eigenvalues is always larger than 1 in magnitude, 1-cycles before the bifurcation are essentially unstable. After the bifurcation point every 1-cycle trajectory has a pair of complex conjugate stability eigenvalues, with absolute value equal to unity with high precision. Of course unity is required, because of noncompressibility of the flow around the fixed point, as proven in [2]. A "test point" started close to a periodic orbit doesn't wander, but always stays bound within an oval surface, probably bacause the invariant torus, on which it lies is still not destroyed by a perturbation. We may consider the σ_- flow as a perturbation. For comparison with corresponding 2-cycles in the figure 10 we observe that 1-cycle of the same map is more stable than 2-cycle. We plotted two trjectories in a region after the bifurcation point.

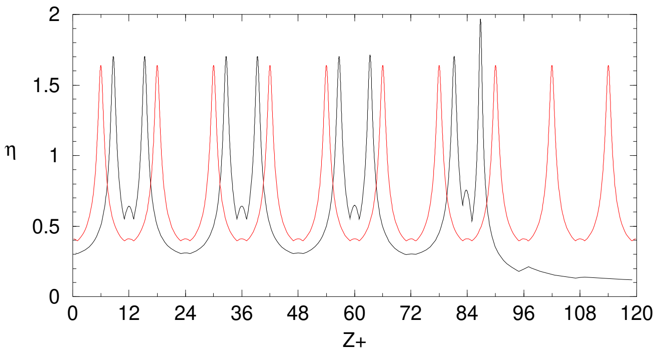

FIG. 10. Periodic trajectories in η. The parameters are $Z_- = 1$ and $Z_+ = 5$, so that period is $T_Z = 12$, 10 periods are plotted. The 1-cycle and the 2-cycle are shown. Initial values were given with the same accuracy. The 1-cycle evidently is more stable.

The next table shows results for 1-cycles calculated for parameter values slightly below and above the bifurcation point. We have put parameter Z_+, a fixed point of 1-cycle η_*, absolute values of stabilities $|\lambda_1|$ and $|\lambda_2|$ and their corresponding real and imaginary parts $\Re\lambda, \Im\lambda$. The absolute values of stabilities should produce up to one, and closiness to one may serve as an indication of accuracy of the integration routine, which, we must admitt could be improved much more on cost of CPU time.

Z_+	η_*	$\lvert\lambda_1\rvert$	$\lvert\lambda_2\rvert$	$\Re\lambda_1$	$\Im\lambda_1$	$\Re\lambda_2$	$\Im\lambda_2$
2.0	0.7015	1.8174	0.5502	-1.817	0.000	-0.550	0.000
2.5	0.6173	2.1839	0.4579	-2.184	0.000	-0.458	0.000
3.0	0.5570	2.0001	0.5000	-2.000	0.000	-0.500	0.000
3.5	0.5098	0.6442	1.5524	-0.644	0.000	-1.552	0.000
4.0	0.5594	2.8860	0.8818	-2.886	0.000	-0.882	0.000
4.0	0.4097	0.3465	1.1341	-0.346	0.000	-1.134	0.000
4.5	0.4387	1.0000	1.0000	-0.766	-0.643	-0.766	0.643
5.0	0.4109	1.0000	1.0000	-0.620	-0.785	-0.620	0.785
5.5	0.3869	1.0000	1.0000	-0.491	-0.871	-0.491	0.871
6.0	0.3659	1.0000	1.0000	-0.379	-0.925	-0.379	0.925
6.5	0.3474	1.0000	1.0000	-0.280	-0.960	-0.280	0.960

7.0	0.3310	1.0000	1.0000	-0.194	-0.981	-0.194	0.981
7.5	0.3163	1.0000	1.0000	-0.117	-0.993	-0.117	0.993
8.0	0.3030	1.0000	1.0000	-0.049	-0.999	-0.049	0.999
8.5	0.2911	1.0001	1.0001	0.012	-1.000	0.012	1.000
9.0	0.2802	1.0000	1.0000	0.067	-0.998	0.067	0.998
9.5	0.2702	1.0000	1.0000	0.116	-0.993	0.116	0.993
10.0	0.2610	1.0000	1.0000	0.160	-0.987	0.160	0.987
10.5	0.2526	1.0000	1.0000	0.201	-0.980	0.201	0.980
11.0	0.2448	1.0000	1.0000	0.238	-0.971	0.238	0.971
11.5	0.2375	1.0000	1.0000	0.272	-0.962	0.272	0.962

TABLE II. Data for 1-cycles around the first bifurcation point.

We have traced out stabilities of 2-cycles ever since they appeared around $Z_+ \approx 3.5$ until about $Z_+ = 12$ and found that stabilities are real. The next bifurcation point was not reached. Still we may anticipate that scenario of period doubling will go in the same way, and we may classify our map as having inverse period doubling bifurcations. For details see e.g. [5]. Through the bifurcation, period one algebraically unstable orbit transits to a stable 1-cycle, producing two also algebraically unstable period two cycles[3]. For algebraical instability one may check [4].

The following table shows analogical data for period two cycles. We put two fixed points and their stabilities after one period, so that actual eigenvalue should be a product of two values.

Z_+	η_*	$\|\lambda_1\|$	$\|\lambda_2\|$	$\Re\lambda_1$	$\Im\lambda_1$	$\Re\lambda_2$	$\Im\lambda_2$
4.0	0.4098	0.3461	1.1342	-0.346	0.000	-1.134	0.000
4.0	0.5595	2.8825	0.8821	-2.883	0.000	-0.882	0.000
5.0	0.3117	0.0858	1.3341	-0.086	0.000	-1.334	0.000
5.0	0.6419	11.6735	0.7490	-11.674	0.000	-0.749	0.000
6.0	0.2630	1.4442	0.0402	-1.444	0.000	-0.040	0.000
6.0	0.6792	0.6912	24.9817	-0.691	0.000	-24.982	0.000
7.0	0.2307	1.5183	0.0232	-1.518	0.000	-0.023	0.000
7.0	0.7028	0.6568	43.2465	-0.657	0.000	-43.246	0.000
8.0	0.2070	1.5714	0.0151	-1.571	0.000	-0.015	0.000
8.0	0.7197	0.6337	66.7137	-0.634	0.000	-66.714	0.000
9.0	0.1886	1.6111	0.0106	-1.611	0.000	-0.011	0.000
9.0	0.7324	0.6172	95.5360	-0.617	0.000	-95.536	0.000
10.0	0.1739	1.6417	0.0078	-1.642	0.000	-0.008	0.000
10.0	0.7425	0.6049	129.8209	-0.605	0.000	-129.821	0.000
11.0	0.1618	1.6654	0.0060	-1.665	0.000	-0.006	0.000
11.0	0.7507	0.5952	169.7422	-0.595	0.000	-169.742	0.000
12.0	0.1515	1.6844	0.0047	-1.684	0.000	-0.005	0.000
12.0	0.7575	0.5874	215.4146	-0.587	0.000	-215.415	0.000

TABLE III. Data for 2-cycles after the first bifurcation point.

[3]Here we have treated terms "period one orbit" and "1-cycle" as synonims.

In the region of the first 1-cycle we have found a bifurcation point, which appears to be inverse, found corresponding 1-cycles and 2-cycles emerging from this point.

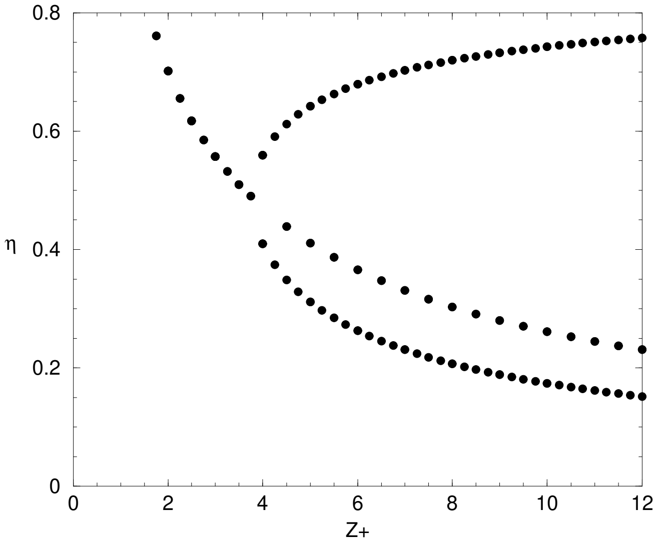

FIG. 11. Period doubling bifurcation diagram. This period doubling bifurcation is inverse.

According to our previous predictions starting from about $Z_+ \approx 14.0$ there is a bifurcation in the sense that another 1-cycle appears. We have found one of them and for illustration we have plotted both of the 1-cycles in some parameter region. The "secondary" 1-cycle has two spikes within the period, thus resembling a 2-cycle. It is unstable in this case, but should gain stability after bifurcation.

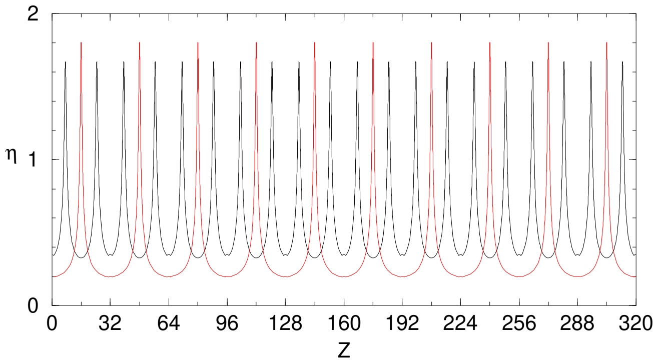

FIG. 12. Two 1-cycles for parameter $Z_+ = 15$. The "secondary" 1-cycle has two spikes within one period. Period $T_Z = 32$. This 1-cycle is less stable than the "primary", it decomposes completely within next ten periods.

In the next table we have displayed some data concerning one of the "secondary" 1-cycle fixed points[4]. We may observe that in the interval $16 < \eta_* < 17$ the stabilities change from real to complex ones. This may be stated as an evidence that there is a bifurcation in this interval.

Z_+	η_*	$\|\lambda_1\|$	$\|\lambda_2\|$	$\Re\lambda_1$	$\Im\lambda_1$	$\Re\lambda_2$	$\Im\lambda_2$
15.0	0.351371	0.2175	4.5970	0.2175	0.0000	4.5970	0.0000

[4]The structure of this table is identical to the structure of the table II

16.0	0.147643	0.8917	3.4326	-0.8917	0.0000	-3.4326	0.0000
17.0	0.182121	1.0000	1.0000	-0.4721	-0.8815	-0.4721	0.8815
18.0	0.175155	1.0000	1.0000	-0.4128	-0.9108	-0.4128	0.9108
19.0	0.168808	1.0000	1.0000	-0.3571	-0.9341	-0.3571	0.9341
20.0	0.162996	1.0000	1.0000	-0.3049	-0.9524	-0.3049	0.9524
21.0	0.157653	1.0000	1.0000	-0.2560	-0.9667	-0.2560	0.9667
22.0	0.152720	1.0000	1.0000	-0.2102	-0.9777	-0.2102	0.9777

TABLE IV. Data for 1-cycles of the second "branch" around their bifurcation point.

In this term paper we have in short discussed some features of one particular nonlinear dynamics. We have discussed many of the results in the [2], also made a little contribution to understanding of this dynamics by producing more accurate Poincaré maps, by finding some of the periodic orbits, their stabilities and also bifurcation points. We have derived a method of finding periodic orbits, which helped us to program routine to finds periodic orbits, and make a short bifurcation analysis.

---

[1] J. Nathan Kutz and Phillip Holmes, “Hamiltonian dynamics of dispersion-managed breathers” J. Opt. Soc. Am. B **299**, 189 (1997).

[2] P.J. Holmes and J.N. Kutz, “Dynamics and bifurcations of a planar map modelling dispersion managed breathers”,`http://www.amath.washington.edu/ kutz/cv.html`

[3] “Classical and Quantum Chaos. A cyclist’s treatise”, Predrag Cvitanović, `http://www.nbi.dk/ChaosBook/`

[4] Jorge V. José, Eugene J. Saletan, “Classical dynamics”, Cambridge university press, 1998

[5] E. Ott, “Chaos in dynamical systems”, Cambridge university press,1993